STRUCTURAL JOINT INVERSION OF ELECTRICAL AND SEISMIC TOMOGRAPHY DATA

L. Palladini, M. Cercato
"Sapienza", DICEA - University of Rome, Italy

Introduction. Groundwater modeling requires the knowledge of aquifer properties, generally derived from direct sampling and laboratory experiments, which are only capable of investigating small volumes of soils and cannot represent the on-site conditions (due to scaling effects, differences in confining pressure, etc). Geophysical methods can help in the reconstruction of a representative hydrologic model of the subsoil since they investigate a much greater volume of the subsurface, are able to image the complexity and heterogeneity of the subsurface itself and provide a continuous model of it (Doetsch *et al.*, 2010). Neverthless, they leave some ambiguities in the reconstruction of the subsoil features, because of the nonuniqueness which is inherent of the inversion process (Doetsch *et al.*, 2010; Moorkamp, 2017).

The joint inversion of two or several geophysical methods, defined as the approach in which different types of data are inverted “within a single algorithm, with a single objective function...” (Moorkamp, 2017) can improve the reconstruction of the subsoil. The reason for this improvement is straightforward: since the various geophysical methods are sensitive to different physical properties, their integration can bring much more confidence in the estimated models. Joint inversion can be conducted using an explicit petrophysical relationship, even if it depends on many physical parameters that vary in the space and cannot be known precisely, or imposing structural similarity between models. Specifically, Gallardo and Meju (2004) developed a structural approach in which the vector cross-product of the gradients of two different models is forced to be zero at each iteration of the inversion, implying similar directions of the gradient vectors (Doetsch *et al.*, 2010). This method has been widely used and slightly modified by various authors (Linde *et al.*, 2006; Demirci *et al.*, 2017) and it is considered one of the most robust methods in the joint inversion of near surface geophysical field data (Linde et Doetsch, 2016).

In this work, we present the joint inversion of Electrical Resistivity Tomography (ERT) and Seismic Refraction Tomography (SRT). The choice of the two geophysical methods is due to their high resolution for the characterization of the shallow subsurface, that is important from an engineering and environmental point of view.

Joint inversion algorithm

Before the description of the joint inversion, we present the inversion methods of individual data set. First, the investigated area is divided in cells, using an uniform regular grid. The forward modelings, $f(\boldsymbol{m})$, for the examined geophysical methods are both nonlinear and consequently approximated with numerical methods. For the electrical method, the Poisson’s equation, that describes the electric field behavior, can be approximated through the finite elements method (Rücker, 2011), while for the seismic method, the eikonal equation can be approximated through the finite-difference scheme of Sethian (1999) (implemented in the pyGIMLi package (Rücker *et al.*, 2017)). The inverse problem can be solved as an optimization problem, in which an objective function is formulated (Gunther, 2004):

$$= {}_d + \lambda {}_m = \left\| D\big(d - f(\boldsymbol{m})\big) \right\|_2^2 + \lambda \left\| C\big(\boldsymbol{m} - \boldsymbol{m}_0\big) \right\|_2^2 \rightarrow min \tag{1}$$

where: d is the vector of field data, whose noise is taken into account in matrix D; $f(\boldsymbol{m})$ is the vector of predicted or synthetic data; C is the constraint matrix; $\boldsymbol{m}$ is the model vector; $\boldsymbol{m}_0$ the reference model vector and λ the regularization parameter that weights the regularization term and is a trade-off parameter between the two terms (Gunther, 2004). Furthermore, Φ_d is called data misfit, while Φ_m the regularization term.

The cross-gradients function, developed and used in the joint inversion of two geophysical methods by Gallardo and Meju (2003, 2004) is defined as the cross product of the gradient vectors of two models, m_1 and m_2, which in our work are m_{ERT} and m_{SRT} respectively:

$$\vec{t}\,(x, y, z) = \nabla m_1(x, y, z) \times \nabla m_2(x, y, z) \tag{2}$$

Adding the cross-gradients function to the objective function, we obtain:

$$(m_1, m_2) = \left\| \begin{matrix} D_1(f(\boldsymbol{m}_1) - d_{obs1}) \\ D_2(f(\boldsymbol{m}_2) - d_{obs2}) \end{matrix} \right\|_2^2 + {}^{1}_{2} \left\| \begin{matrix} C(\boldsymbol{m}_1 - \boldsymbol{m}_{01}) \\ C(\boldsymbol{m}_2 - \boldsymbol{m}_{02}) \end{matrix} \right\|_2^2 + {}_{cg} \left\| t(\boldsymbol{m}_1, \boldsymbol{m}_2) - t_0 \right\|_2^2 \rightarrow min \tag{3}$$

in which t and t_0 are the cross-gradients function and its a priori value respectively and λ_{CG} is the regularization parameter that weights the cross-gradients function. In order to minimize the objective function, in a first attempt the Gauss-Newton method (Gunther, 2004) was used writing the model update as:

$$\left\{ \begin{bmatrix} S_1^T D_1^T D_1 S_1 & 0 \\ 0 & S_2^T D_2^T D_2 S_2 \end{bmatrix} + \begin{bmatrix} \lambda_1 C^T C & 0 \\ 0 & \lambda_2 C^T C \end{bmatrix} + \lambda_{CG} \begin{bmatrix} B_1^T B_1 & B_1^T B_2 \\ B_2^T B_1 & B_2^T B_2 \end{bmatrix} \right\} \cdot \begin{bmatrix} \Delta m_1 \\ \Delta m_2 \end{bmatrix} = \begin{bmatrix} S_1^T D_1^T D_1 (d_{obs1} - f_1(m_1)) \\ S_2^T D_2^T D_2 (d_{obs2} - f_2(m_2)) \end{bmatrix} - \begin{bmatrix} \lambda_1 C^T C (m_1 - m_{01}) \\ \lambda_2 C^T C (m_2 - m_{02}) \end{bmatrix} - \lambda_{CG} \begin{bmatrix} B_1^T \left(t(m_1, m_2) - t_0 \right) \\ B_2^T \left(t(m_1, m_2) - t_0 \right) \end{bmatrix} \quad (4)$$

where S_1 and S_2 are the jacobian matrices for the two methods, and B_1 and B_2 are the jacobian matrices associated with the cross-gradient function. Because of the high number of model parameters, the system of equations (4) has been iteratively solved using the conjugate gradient method (Gunther, 2004).

Field data. The field data have been acquired with the aim of characterizing the shallow subsurface around and below a historic building situated near Rieti (Central Italy). The construction, built in 1910 as a two-floor masonry building and now used as a National research centre for agricultural studies (Fig.1a), exhibits some fractures on the load-bearing walls and possible differential settlements phenomena in the soil foundations.

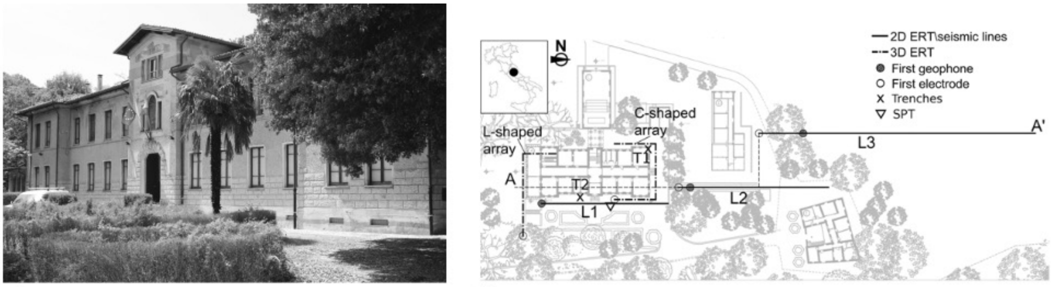

a) b)

Fig. 1 - a) Photograph of the historical building; b) location of geophysical and geotechnical measurements (Cercato and De Donno, 2018).

The area is situated "within a travertine outcropping area, with variable soil thickness above the travertine bedrock" (Cercato and De Donno, 2018). Different types of geophysical measurements were conducted on the site (Fig. 1b), but we will focus on the L3 line, which allows the reconstruction of the shallow subsoil near the building. The ERT measurements were acquired with a 48-electrodes IRIS Instruments SyscalPro48 using a combination of dipole-dipole and Wenner-Schlumberger configurations with stainless steel electrodes 2m spaced apart, while the SRT data using a 48-channel system of 4.5 Hz vertical geophones 1m spaced (we examined the P-wave data) and a 7 kg hammer on a steel plate as source, with a Geometrics Geode seismograph at a sampling rate of 0.125ms.

Results. In a first attempt, the ERT and SRT data were inverted separately. In order to choose the optimal value of λ for the inversion, the L- curve (Zhdanov, 2015) was constructed both for ERT and SRT (Fig. 2a,b).

The ERT convergence was reached after 4 iterations, while the SRT after 5 iterations. The ERT section (Fig. 3a) showed three different layers: the conductive one with values of resistivity <20Ωm for the shallower and in the range of 30-60Ωm for the middle one, and a deeper resistive layer, in the left part of the section, with a resistivity >100Ω·m, that probably represents a travertinous formation. The SRT map (Fig. 3b) confirms the ERT map results, since a first layer with low P-wave, with velocities in the range of 300-600m/s is individuated. These values are typical of a weathered layer. Then, velocities increase with depth, reaching values >800m/s for the middle layer and >1000m/s in the left part of the section in a position that overlaps the one of the ERT map. These high velocities (>1000m/s) suggest the presence of a travertineous

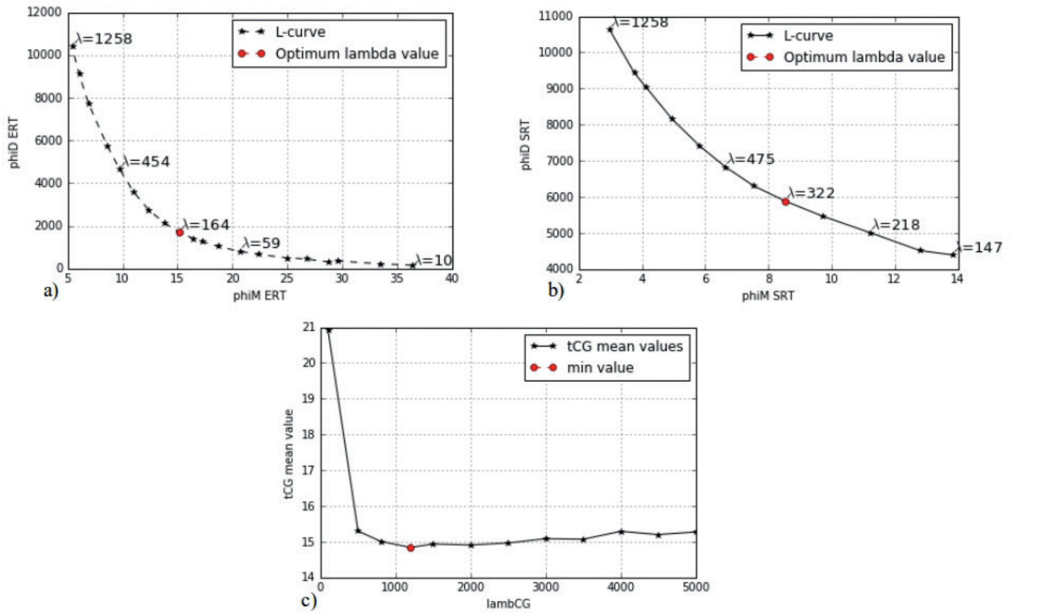

Fig. 2 - a) L-curve for ERT data; b) L-curve for SRT data; c) Graph of the mean value of the cross-gradients function for the field data.

layer, visible only in the left part of the section, because of the maximum depth of 10m that is reached by the SRT inversion. The map of the cross-gradients function (Fig. 3c) obtained from the ERT and SRT inverted models and calculated using the forward difference scheme with uniform discretization, exhibits a few areas of structural difference in the left part of the section, with values around zero in the most of the section. The scatter-plot (Fig. 3d) shows a certain dispersion of data, typical of field data, which are affected by some errors.

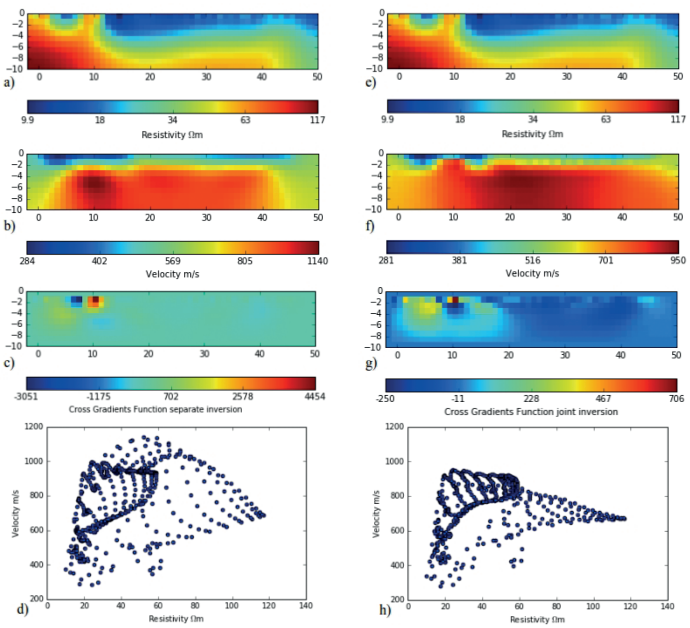

Fig. 3 - a) ERT map obtained from the separated inversion; b) SRT map obtained from the separated inversion; c) Map of the cross-gradients function for the separated inversion; d) Scatter plot for the separated inversion; e) ERT map obtained from the joint inversion; f) SRT map obtained from the joint inversion; g) Map of the cross-gradients function for the joint inversion; h) Scatter plot for the joint inversion.

The joint inversion was conducted using the lambda values and the same conditions of the separated inversion, choosing the λ_{CG} value as the minimum mean value of the cross-gradients vector and specifically 1200 (Fig. 2c). The convergence was reached after 5 iterations. ERT map is very similar to the one obtained by the separated inversion (Fig. 3e), while the

SRT map (Fig. 3f) shows some differences: it individuates the presence of the first layer, with velocities in the range of 300-600m/s, and of a second layer, with higher velocity, between 700 and 900m/s, as in the separated inversion, but since the maximum reached value is 950m/s, the travertinous area seems not to be individuated.

However, the significant maps for the joint inversion, as the map of the cross-gradients function and the scatter plot, show the good results obtained. The map of the cross-gradients function (Fig. 3g) shows a remarkable reduction, meaning that the two models have a better structural similarity than the separated inversion and the scatter-plot (Fig. 3h) highlights a reduced data dispersion, even if it is not possible to define more defined sublayering probably because of the errors in data.

In conclusion, the joint inversion is capable, through the cross-gradient operator, of improving the consistency between the two different models without the need to use a specific relationship between the resistivity and seismic velocity, reducing the ambiguities in the interpretation of the joint inversion subsoil model.

References

Cercato M. and G. De Donno; 2018: *Focusing on soil-foundation heterogeneity through high-resolution electrical and seismic tomography*. Near Surface Geophysics 16 (1), 1-12

Demirci I.˙, Candansayar M.E., Vafidis A.., Soupios P.; 2017: *Two dimensional joint inversion of direct current resistivity, radio-magnetotelluric and seismic refraction data: an application from Bafra Plain, Turkey*. J Appl Geophys 139:316–330.

Doetsch J., Linde N., Coscia I., Greenhalgh S. A., and Green A. G.; 2010: *Zonation for 3D aquifer characterization based on joint inversions of multimethod crosshole geophysical data*. Geophysics, 75, no. 6, G53–G64,doi: 10.1190/1.3496476.

Gallardo L. A., and Meju M. A..; 2004: *Joint two-dimensional DC resistivity and seismic travel time inversion with cross gradients constraints*. J. Geophys. Res., 109, B03311, doi:10.1029/2003JB002716.

Günther T.; 2004: *Inversion Methods and Resolution Analysis for the 2D/3D Reconstruction of Resistivity Structures from DC Measurements*, PhD thesis, Freiberg University of Mining and Technology.

Linde N., Binley A., Tryggvason A., Pedersen L. B., and Revil A.; 2006: *Improved hydrogeophysical characterization using joint inversion of cross-hole electrical resistance and ground-penetrating radar traveltime data*. Water Resour. Res., 42, W12404, doi:10.1029/2006WR005131.

Linde N. and Doetsch J.; 2016: *Joint inversion in hydrogeophysics and near-surface geophysics*. In: Integrated imaging of the Earth, M. Moorkamp, P. Lelievre, N. Linde, and A. Khan (Editors), ch.7, 119-135, John Wiley & Sons, Inc. Hoboken, New Jersey. Doi: 10.1002/9781118929063.ch7.

Moorkamp M.; 2017: *Integrating electromagnetic data with other geophysical observations for enhanced imaging of the earth: a tutorial and review*. SurvGeophys. doi:10.1007/s10712-017-9413-7.

Rücker C.; 2011: *Advanced Electrical Resistivity Modelling and Inversion using Unstructured Discretization*. PhD thesis, University of Leipzig

Rücker C., Günther, T., Wagner, F.M.; 2017: *pyGIMLi: An open-source library for modelling and inversion in geophysics*. Computers and Geosciences, 109, 106-123, doi: 10.1016/j.cageo.2017.07.011.

Sethian J.A.; 1999: *Fast marching methods*. SIAMRev., Vol. 41,No. 2, pp. 199–235.

Zhdanov M.S.; 2015: *Inverse Theory and Applications in Geophysics*, Elsevier Published.